J. Fluid Mech. (1990), *vol.* 214, *pp.* 535–557
Printed in Great Britain

Relative dispersion in two-dimensional turbulence

By A. BABIANO, C. BASDEVANT, P. LE ROY AND R. SADOURNY

Laboratoire de Météorologie Dynamique, Ecole Normale Supérieure, Paris Cedex 05, France

(Received 1 June 1988 and in revised form 16 October 1989)

In this paper we study the statistical laws of relative dispersion in two-dimensional turbulence by deriving an exact equation governing its evolution in time, then evaluating the magnitude of its various terms in numerical experiments, which allows us to check the validity of the classical dispersion laws: the equivalent to the Richardson–Obukhov t^3 law in the energy cascade range, and the Kraichnan–Lin exponential law in the enstrophy cascade range. We examine theoretically and experimentally the conditions of validity of both laws. It is found that the t^3 law is obtained in the energy inertial range provided the separation scale of the particles is smaller by an order of magnitude than the injection scale. When the t^3 law is reached, the relative acceleration correlations are observed to have reached a statistical quasi-stationary stage: this would tend to justify in the energy inertial range of two-dimensional turbulence a working hypothesis formulated by Lin & Reid (1963); also, the necessity of starting from very small initial separations to get the t^3 law may be explained by the time necessary for relative acceleration correlations to reach the statistical quasi-stationary regime. On the other hand, the Kraichnan–Lin exponential law is, strictly speaking, never observed; it is in fact reduced to a very short transient stage when the relative dispersion characteristic time reaches its minimum value, as predicted by Batchelor.

1. Introduction

The fundamental results on turbulent relative dispersion are essentially derived from Batchelor's work as well as from a number of approaches inspired by Kolmogorov's and Obukhov's self-similarity theory (Batchelor 1952; Obukhov 1941): for extensive reviews see Monin & Yaglom (1975) and Bennett (1987). In the case of two-dimensional turbulence, these classic approaches result in the following behaviour for the relative dispersion coefficient (Kraichnan 1966; Lin 1972; Bennett 1984):

$$\frac{1}{2}\frac{\mathrm{d}}{\mathrm{d}t}D^2 \sim D^{\frac{4}{3}} \quad \text{in the energy cascade,} \tag{1a}$$

$$\frac{1}{2}\frac{\mathrm{d}}{\mathrm{d}t}D^2 \sim D^2 \quad \text{in the enstrophy cascade.} \tag{1b}$$

The $\frac{4}{3}$-exponent law or Richardson–Obukhov law (R–O hereafter) corresponds to a cubic growth with time of the mean-squared relative displacement D^2:

$$D^2 \sim t^3 \quad \text{in the energy cascade,} \tag{2a}$$

while the 2-exponent law or Kraichnan–Lin law (K–L hereafter) corresponds to an exponential growth:

$$D^2 \sim \exp\left[c\frac{t}{\tau_*}\right] \quad \text{in the enstrophy cascade.} \tag{2b}$$

Here c is a non-dimensional constant and τ_* the characteristic dispersion time, defined by the enstrophy cascade rate or by enstrophy in local or non-local cases respectively. Let us recall that in the framework of the self-similarity theory, dynamics are said to be non-local when contributions to the evolution of a given scale come mainly from scales much larger than it. Conversely in local dynamics a given scale interacts principally with comparable scales. A good physical illustration of local and non-local concepts for turbulent dispersion can be found in Er-El & Peskin (1981). The classic results (1a, b) or derived results R–O and K–L (2a, b) have been qualitatively confirmed through the experiments of Morel & Larchevêque (1974) and Er-El & Peskin (1981) in the atmosphere, and Price (1981) and the experiments summarized in Okubo (1971) and Anikiev *et al.* (1985) in the ocean.

In two previous articles, Babiano, Basdevant & Sadourny (1985), Babiano *et al.* (1987), referred to hereinafter as (BBS and BBLS), we re-examined, in the particular context of two-dimensional incompressible turbulence, the relative and single-particle dispersion laws, and their links with the scale dependency of Eulerian and Lagrangian energy spectra. The objective of the following work is to complete the analyses developed in BBS concerning the relative dispersion, and to give theoretical formulations whose verification by direct numerical experimentation can be done in a relatively simple manner. We shall analyse the K–L law from the standpoint of Bachelor's (1952a, b) classical analyses. Concerning the R–O law, we shall show that, in two-dimensional turbulence, the scales of the inverse cascade of energy are reached after dispersion times long enough to allow the use of Lin & Reid's (1963) hypotheses on stationarity of the correlations of relative accelerations. This assumption is not in general natural to the concept of relative dispersion; however, in the energy inertial range of two-dimensional turbulence, these working hypotheses appears not too unrealistic.

After a quick review (§2) of the results given in BBS and BBLS, we shall show in §3 how the relative dispersion law can be formulated as a kinematic equation; the classic results R–O and K–L will then be compared to both solutions of this kinematic equation and results from numerical experiments. In §§4 and 5 we shall examine the sufficient conditions to enable R–O and K–L to be observed.

The Eulerian numerical simulation and the Lagrangian experiments are described in the Appendix.

2. Definitions and background

2.1. *Definitions*

We are interested in the dispersion of particle pairs which, initially separated by a given distance $D_0 = \|\boldsymbol{D}_0\|$, are advected by stationary two-dimensional turbulence. For every pair of particles with Lagrangian coordinates $\boldsymbol{a}_1$ and $\boldsymbol{a}_2$ ($\boldsymbol{D}_0 = \boldsymbol{a}_1 - \boldsymbol{a}_2$), the separation vector $\boldsymbol{D}$ at time t is expressed through $\boldsymbol{D}_0$ and the absolute displacement vector $\boldsymbol{A}$ by

$$\boldsymbol{D}(t, \boldsymbol{D}_0) = \boldsymbol{D}_0 + [\boldsymbol{A}(\boldsymbol{a}_1, t) - \boldsymbol{A}(\boldsymbol{a}_2, t)],$$

where $\boldsymbol{A}$ is defined in terms of the Lagrangian velocity field $\boldsymbol{V}$ by

$$\boldsymbol{A}(\boldsymbol{a}, t) = \int_0^t \boldsymbol{V}(\boldsymbol{a}, \tau)\, \mathrm{d}\tau. \tag{3}$$

Defining the Lagrangian relative velocity vector $\delta \boldsymbol{V} = \mathrm{d}/\mathrm{d}t\, \boldsymbol{D}$ and the relative acceleration vector $\delta \boldsymbol{\Gamma} = \mathrm{d}/\mathrm{d}t\, \delta \boldsymbol{V}$, one can write

$$\boldsymbol{D}(t, \boldsymbol{D}_0) = \boldsymbol{D}_0 + \int_0^t \delta \boldsymbol{V}(\tau, \boldsymbol{D}_0)\, \mathrm{d}\tau, \tag{4}$$

$$\delta \boldsymbol{V}(t, \boldsymbol{D}_0) = \delta \boldsymbol{V}_0 + \int_0^t \delta \boldsymbol{\Gamma}(\tau, \boldsymbol{D}_0)\, \mathrm{d}\tau. \tag{5}$$

Denoting by $\langle \cdot \rangle_a$ the ensemble average at time t over all particles and by $\langle \cdot \rangle$ the ensemble average at time t over all particles pairs initially separated by a given distance D_0, the single-particle dispersion and the relative dispersion are defined by

$$A^2(t) = \langle \boldsymbol{A}(\boldsymbol{a}, t) \cdot \boldsymbol{A}(\boldsymbol{a}, t) \rangle_a, \tag{6}$$

$$D^2(t, D_0) = \langle \boldsymbol{D}(t) \cdot \boldsymbol{D}(t) \rangle. \tag{7}$$

The absolute and relative dispersion coefficients $K(t)$ and $Y(t, D_0)$ are defined by

$$K(t) = \frac{1}{2} \frac{\mathrm{d}}{\mathrm{d}t} A^2(t) = \langle \boldsymbol{A}(\boldsymbol{a}, t) \cdot \boldsymbol{V}(\boldsymbol{a}, t) \rangle_a, \tag{8}$$

$$Y(t, D_0) = \frac{1}{2} \frac{\mathrm{d}}{\mathrm{d}t} D^2(t, D_0) = \langle \boldsymbol{D}(t, \boldsymbol{D}_0) \cdot \delta \boldsymbol{V}(t, \boldsymbol{D}_0) \rangle. \tag{9}$$

Using (8) and (3) we obtain

$$K(t) = \int_0^t \langle \boldsymbol{V}(\boldsymbol{a}, t) \cdot \boldsymbol{V}(\boldsymbol{a}, \tau) \rangle_a \, \mathrm{d}\tau; \tag{10}$$

similarly from (9) and (4)

$$Y(t, D_0) = \langle \boldsymbol{D}_0 \cdot \delta \boldsymbol{V}(t, \boldsymbol{D}_0) \rangle + \int_0^t \langle \delta \boldsymbol{V}(t, \boldsymbol{D}_0) \cdot \delta \boldsymbol{V}(\tau, \boldsymbol{D}_0) \rangle \, \mathrm{d}\tau. \tag{11}$$

Hypothesis H1: If the turbulence is homogeneous the following condition is verified:

$$\langle \boldsymbol{D}_0 \cdot \delta \boldsymbol{V}(t, \boldsymbol{D}_0) \rangle = 0.$$

Assuming condition H1 and using (10), (11) can be expanded into

$$Y(t, D_0) = 2K(t) - 2 \int_0^t \langle \boldsymbol{V}(\boldsymbol{a}_1, t) \cdot \boldsymbol{V}(\boldsymbol{a}_2, \tau) \rangle \, \mathrm{d}\tau. \tag{12}$$

Figure 1 (*a*) shows typical behaviour of $Y(t)$ and $2K(t)$. The times T_I and T_E are the times necessary for relative dispersion (7) to reach respectively the forcing scale D_I or the most energetic scale D_E (see table 1); they are functions of D_0. The time T_Z is defined by $T_Z = Z^{-\frac{1}{2}}$, where $Z = \frac{1}{2} \langle \| \mathrm{curl}\, \boldsymbol{V} \|^2 \rangle_x$ is the enstrophy of the flow, $\langle \cdot \rangle_x$ referring to averaging over all Eulerian position vectors $\boldsymbol{x}$. We observe from figure 1 (*a*) that $Y(t)$ and $2K(t)$ depend linearly on t for $t \leqslant T_Z$, and become practically constant and identical to each other for $t \geqslant T_E$. The latter behaviour is consistent with the vanishing of the correlation term in (12) at large times, when the separation scale becomes larger than the most energetic scale. Figure 1 (*b*) shows the first correlation term in (11): $\langle \boldsymbol{D}_0 \cdot \delta \boldsymbol{V} \rangle$. H1 is well verified in our numerical experiment R256F40 (see Appendix for details) when the statistical sampling is performed over 1024 pairs (curve 1); when the sampling is downgraded to 128 pairs (an estimate closer to practical capabilities of *in situ* or laboratory observations) H1 is verified

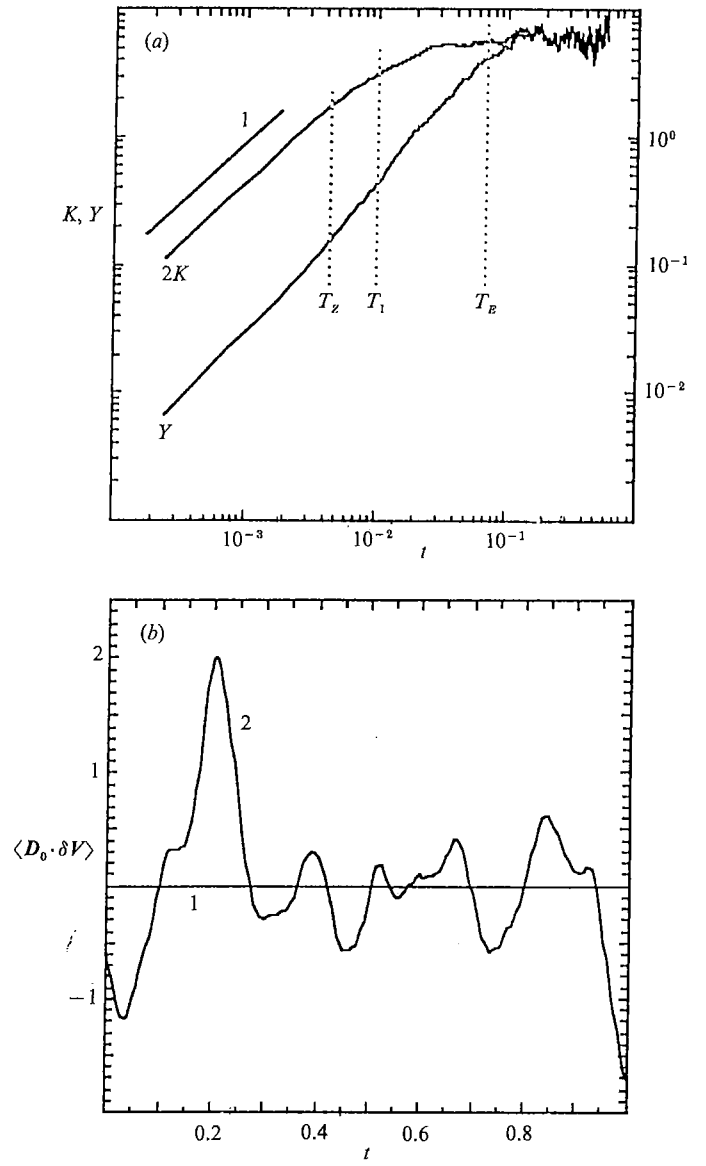

FIGURE 1. (*a*) Behaviour of dispersion coefficients K and Y as a function of time. (*b*) The correlation term $\langle D_0 \cdot \delta V \rangle$; curve 1, corresponding to 1024 pairs, is indistinguishable from the time axis; curve 2 corresponds to 128 pairs.

only in the time-mean sense (curve 2). Thus, in practical experiments, a significant level of noise is to be expected when verifying (12).

Single-particle dispersion (6), (10) can be studied theoretically within the framework of Taylor's and Batchelor's analyses, based on its rigorous relation with the Lagrangian energy spectrum $L(\nu)$. This kind of approach, however, is less well suited to relative dispersion, because the velocity correlation in (11) or the cross-correlation in (12) are not stationary (they depend both on t and τ) and cannot be rigorously related, either to $L(\nu)$, or to the Eulerian energy spectrum $E(k)$. Kraichnan (1966) and Bennett (1984) give a spectral analysis of (12) introducing the concept of

	t^* (days)	l^* (km)	E	Z	T_L	T_Z	D_I	D_E
R256F40	553.8	636.6	113	57000	0.013	0.0042	0.0785	0.4
R1024F40	555.05	636.6	113.5	75800	0.0125	0.0036	0.0785	0.35
R1728F40	557.5	636.6	114.5	66500	0.0115	0.0039	0.0785	0.35
R1024F4	102.2	63.66	15.4	241.8	0.08	0.064	0.785	—

TABLE 1. Characteristic non-dimensional parameters of the experiments

Lagrangian modal time correlation defined in homogeneous two-dimensional turbulence as

$$R(k,\tau) = U(k,\tau)/U(k,0), \tag{13}$$

with
$$\left.\begin{aligned} U(k,\tau) &= (2\pi)^{-2}\int \exp(\mathrm{i}\boldsymbol{k}\cdot\boldsymbol{D})\,\overline{\boldsymbol{V}(\boldsymbol{x}+\boldsymbol{D},t)\cdot\boldsymbol{V}(\boldsymbol{x},t\,|\,t-\tau)}\,\mathrm{d}^2\boldsymbol{D}, \\ U(k,0) &= (2\pi k)^{-1}E(k). \end{aligned}\right\} \tag{14}$$

In (14), $\boldsymbol{V}(\boldsymbol{x},t\,|\,t-\tau)$ is the velocity at time $t-\tau$ of a particle whose position at time t is $\boldsymbol{x}$; the bar refers to averaging with respect to $\boldsymbol{x}$. Bennett (1984) rightly mentions that (14), contrary to (12), is not a strictly Lagrangian description; it does not allow particle pairs which were originally separated by a given D_0 from each other to be distinguished. In this case, it is simpler and more convenient to use instead of (12) and (14), the instantaneous relative dispersion coefficient

$$X(\mathscr{D}) = \left\{\left\langle\left[\frac{1}{2}\frac{\mathrm{d}}{\mathrm{d}t}\boldsymbol{D}\cdot\boldsymbol{D}\right]^2\right\rangle_{\mathscr{D}}\right\}^{\frac{1}{2}} = \{\langle[\boldsymbol{D}\cdot\delta\boldsymbol{V}(\boldsymbol{D})]^2\rangle_{\mathscr{D}}\}^{\frac{1}{2}},$$

where $\langle\cdot\rangle_{\mathscr{D}}$ is the conditional ensemble average obtained when $\|\boldsymbol{D}\| = \mathscr{D}$, independently of D_0. The instantaneous relative dispersion coefficient $X(\mathscr{D})$ can be expressed using the second-order longitudinal structure function $S_\parallel(\mathscr{D})$:

$$X(\mathscr{D}) = [S_\parallel(\mathscr{D})]^{\frac{1}{2}}\mathscr{D}. \tag{15}$$

2.2. *Instantaneous relative dispersion*

Instantaneous relative dispersion has been studied in BBS in connection with the Eulerian energy spectrum. The characteristic timescale is defined as

$$\tau_X(\mathscr{D}) = \frac{\mathscr{D}^2}{X(\mathscr{D})}. \tag{16}$$

At small scales, the asymptotic behaviour of X and τ_X is given by

$$X(\mathscr{D}) \approx \tfrac{1}{2}Z^{\frac{1}{2}}\mathscr{D}^2, \quad \tau_X(\mathscr{D}) \approx 2Z^{-\frac{1}{2}} \quad \text{for} \quad \mathscr{D}\to 0. \tag{17}$$

In a range of scales where self-similarity holds for the Eulerian energy spectrum, say $E(k) = k^{-m}$, we have

$$\left.\begin{aligned} &X(\mathscr{D}) \sim \mathscr{D}, \quad \tau_X \sim \mathscr{D} \quad \text{for} \quad 1 \leqslant m, \\ &X(\mathscr{D}) \sim \mathscr{D}^{\frac{m+1}{2}}, \quad \tau_X \sim \mathscr{D}^{\frac{3-m}{2}} \quad \text{for} \quad 1 \leqslant m \leqslant 3, \\ &X(\mathscr{D}) \sim \mathscr{D}^2, \quad \tau_X \sim 2Z^{-\frac{1}{2}} \quad \text{for} \quad m \geqslant 3. \end{aligned}\right\} \tag{18}$$

Expressions (18) are indeed consistent with the classic result ($1a, b$) for $m = \frac{3}{5}$ or $m \geqslant 3$ cases (for an argument based on (12) and the self-similarity assumption, see Bennett 1984). However, $X(\mathscr{D})$ being defined in a root-mean-square sense, (18) cannot be rigorously integrated in time to yield R–O or K–L (($2a$) or ($2b$)).

Two important conclusions can be stated at this stage: first, the asymptotic law (17) established by Taylor expansion at vanishing scales extends in fact throughout the enstrophy inertial range; and secondly, all 'non-local' energy spectra give in practice undistinguishable instantaneous dispersion and structure functions. The latter assumption means that it will be extremely difficult to recover the time energy spectrum, or to make use of a formulation like (14), in the context of studying the enstrophy inertial range by laboratory or *in situ* experiments.

2.3. *Single-particle dispersion*

As in the instantaneous relative dispersion case, the single-particle dispersion (6) and diffusivity (10) can be examined in connection with the shape of the energy spectrum (see BBLS). For a Lagrangian energy spectrum $L(\nu) = \nu^{-n}$ in a Lagrangian frequency domain $\nu_1 \ll \nu \sim 1/t \ll \nu_2$ three cases will be considered:

$$\left.\begin{aligned} &A^2(t) \sim t^2, \quad K(t) \sim t \quad \text{for} \quad n > 1, \\ &A^2(t) \sim t^{n+1}, \quad K(t) \sim t^n \quad \text{for} \quad -1 < n < 1, \\ &A^2(t) \sim \text{const.}, \quad K(t) = 0 \quad \text{for} \quad n < -1. \end{aligned}\right\} \tag{19}$$

Expressions (19) show that $A^2(t)$ and $K(t)$ saturate for $n > 1$ and then no longer depend on the slope of the Lagrangian energy spectrum. In this case again, $L(\nu)$ is difficult to reconstruct and (14) difficult to use in the context of practical experiments.

Taylor–Batchelor's asymptotic behaviour

$$A^2 \sim 2Et^2, \quad K(t) \sim 2Et \tag{20}$$

is more than simply the asymptotic laws for $t \to 0$, as it remains valid in sufficiently general cases ($n > 1$). In (20) E is the mean Lagrangian kinetic energy, defined as $E = \frac{1}{2}\langle \|V\|^2 \rangle_a$. The validity of (20) is commonly accepted for $t \ll T_L$, where T_L is the Lagrangian integral timescale. Assuming that the Lagrangian correlation is Gaussian in shape, we noticed in BBLS that in homogeneous and isotropic two-dimensional turbulence, T_L is given by

$$T_L \approx (2\pi/3)^{\frac{1}{2}} Z^{-\frac{1}{2}} = 1.45\, T_Z. \tag{21}$$

Experimental results shown in figure 1 (*a*) and later indicate that (20) remains valid up to $t = T_Z$.

2.4. *The case of inhomogeneous flows*

It is customary to express the characteristic nonlinear timescale as the inverse square root of the enstrophy: this type of formulation has been used in (17). Strictly speaking however, the Taylor expansion of velocity used in the derivation of (17) yields a first-order estimate of the longitudinal structure function which involves the velocity gradient rather than vorticity. The corresponding expression for $X(\mathscr{D})$ is

$$X(\mathscr{D}) \approx \tfrac{1}{2}[\tfrac{1}{2}\langle \|\nabla V\|^2 \rangle_x]^{\frac{1}{2}} \mathscr{D}^2 \quad \text{for} \quad \mathscr{D} \to 0.$$

The squared norm of the velocity gradient is generally expressed as

$$\|\nabla V\|^2 = \tfrac{1}{2}(\omega^2 + s_1^2 + s_2^2),$$

where ω refers to vorticity and s_1, s_2 to deformations:

$$\omega = \partial_x v - \partial_y u, \quad s_1 = \partial_x u - \partial_y v, \quad s_2 = \partial_x v + \partial_y u.$$

The $\langle\cdot\rangle_x$ average acting over the whole flow domain, (17) follows from the equalities

$$\langle\|\nabla V\|^2\rangle_x = \langle\omega^2\rangle_x = \langle s_1^2+s_2^2\rangle_x,$$

which hold for adequate boundary conditions such as periodicity or vanishing velocity.

In experimental practice, we may have to consider cases where the set of particles does not sample the whole flow domain, but is restricted to a sub-domain Ω. If, in addition, the flow is inhomogeneous, then (17) and 21) are no longer valid: Z must be replaced by the squared norm of the velocity gradient over Ω.

3. Relative dispersion

3.1. *Theory: a differential equation to govern relative dispersion*

In this section we shall give a mathematical description of relative dispersion following that already explored in Lin (1960), Lin & Reid (1963) and Babiano & Le Roy (1987). From (4), we get (for simplicity we shall omit reference to the dependency on D_0 in all the following expressions)

$$\|\boldsymbol{D}-\boldsymbol{D}_0\|^2 = \left\|\int_0^t \delta\boldsymbol{V}(\tau)\,\mathrm{d}\tau\right\|^2,$$

which yields

$$t\frac{\mathrm{d}}{\mathrm{d}t}\|\boldsymbol{D}-\boldsymbol{D}_0\|^2 = 2t\delta\boldsymbol{V}(t)\int_0^t \delta\boldsymbol{V}(\tau)\,\mathrm{d}\tau. \tag{22}$$

On the other hand, an integration by parts yields the identity

$$\int_0^t \delta\boldsymbol{V}(\tau)\,\mathrm{d}\tau = t\delta\boldsymbol{V}(t)-\int_0^t \tau\,\delta\boldsymbol{\Gamma}(\tau)\,\mathrm{d}\tau; \tag{23}$$

hence (22) can be rewritten

$$\begin{aligned} t\frac{\mathrm{d}}{\mathrm{d}t}\|\boldsymbol{D}-\boldsymbol{D}_0\|^2 &= \left[t\delta\boldsymbol{V}(t)+\int_0^t \tau\delta\boldsymbol{\Gamma}(\tau)\,\mathrm{d}\tau+\int_0^t \delta\boldsymbol{V}(\tau)\,\mathrm{d}\tau\right]\cdot\int_0^t \delta\boldsymbol{V}(\tau)\,\mathrm{d}\tau \\ &= \left[t\delta\boldsymbol{V}(t)+\int_0^t \tau\delta\boldsymbol{\Gamma}(\tau)\,\mathrm{d}\tau\right]\cdot\int_0^t \delta\boldsymbol{V}(\tau)\,\mathrm{d}\tau+\|\boldsymbol{D}-\boldsymbol{D}_0\|^2. \end{aligned}$$

Using (23) again:

$$\frac{\mathrm{d}}{\mathrm{d}t}\frac{\|\boldsymbol{D}-\boldsymbol{D}_0\|^2}{t} = \|\delta\boldsymbol{V}(t)\|^2-\left\|\frac{1}{t}\int_0^t \tau\delta\boldsymbol{\Gamma}(\tau)\,\mathrm{d}\tau\right\|^2. \tag{24}$$

Relation (24) is a differential equation which governs the time evolution of the separation $\boldsymbol{D}$ of a particle pair. Averaging (24) over a set of particle pairs initially separated by a given distance D_0 and integrating in time yields

$$\langle\|\boldsymbol{D}-\boldsymbol{D}_0\|^2\rangle = t\int_0^t F(\tau,D_0)\,\mathrm{d}\tau, \tag{25}$$

with

$$F(t,D_0) = \langle\|\delta\boldsymbol{V}(t,\boldsymbol{D}_0)\|^2\rangle-G(t,D_0), \tag{26}$$

$$G(t,D_0) = \left\langle\left\|\frac{1}{t}\int_0^t \tau\delta\boldsymbol{\Gamma}(\tau,\boldsymbol{D}_0)\,\mathrm{d}\tau\right\|^2\right\rangle. \tag{27}$$

Within the limits of hypothesis H1, (25) yields

$$D^2(t,D_0) = D_0^2 + t\int_0^t F(\tau,D_0)\,\mathrm{d}\tau. \tag{28}$$

Equations (25) and (28) have been obtained from strictly kinematic arguments; (25) is rigorous. In both cases the dynamics of the flow acts through the terms $\langle\|\delta V\|^2\rangle$ and G. Equation (25) is a generalization of Lin & Reid's (1963) formulation, and complements (11), over which it has a few advantages: first, (25) and its H1-equivalent (28) clearly separate the respective contributions of velocity and acceleration; secondly, it lends itself more easily than (11) or (12) to developments without reference to self-similarity hypotheses.

3.2. *Asymptotic behaviour of relative dispersion*

At large times, the velocities of the two particles in a pair become decorrelated, so that

$$\langle\|\delta V\|^2\rangle \sim 4E \quad \text{when} \quad t\to\infty. \tag{29}$$

Further, if we assume that the integral of the time correlation of the relative velocities involved in the relation (11) converges, then

$$D^2 \sim t \quad \text{when} \quad t\to\infty, \tag{30}$$

which, together with (29), yields

$$G \sim 4E \quad \text{when} \quad t\to\infty. \tag{31}$$

At small times, if D_0 is a small scale in the enstrophy range, $\langle\|\delta V\|^2\rangle$ is a function of the enstrophy Z, as shown in BBS:

$$\langle\|\delta V\|^2\rangle \sim 2S(D_0) \sim ZD_0^2 \quad \text{when} \quad t\to 0, \tag{32}$$

where $S(\mathscr{D}) = \frac{1}{2}\langle\|\delta V(\boldsymbol{D})\|^2\rangle_{\mathscr{D}}$, is the Eulerian second-order structure function. The only thing we know *a priori* about G is its asymptotic behaviour for $t\to 0$:

$$G \sim \tfrac{1}{4}\langle\|\delta\boldsymbol{\Gamma}_0\|^2\rangle t^2 \quad \text{when} \quad t\to 0. \tag{33}$$

Then the asymptotic behaviour of (28) for small times is

$$D^2(t,D_0) = D_0^2 + 2S(D_0)t^2 \quad \text{when} \quad t\to 0. \tag{34}$$

Relation (34) is well known (see Hinze 1975 and Kraichnan 1966). According to (32) we obtain the two-dimensional variant of (34):

$$D^2(t,D_0) = D_0^2(1+Zt^2) \quad \text{when} \quad t\to 0. \tag{35}$$

As we have demonstrated in §2.3 that (20) is valid in a much larger interval than the vicinity of $t\to 0$, we shall now show that the asymptotic law (35) can be extended to a similar frequency range. From (12) and definition (3),

$$Y(t,D_0) = 2K(t) - 2\Theta, \tag{36}$$

with

$$\Theta = \int_0^t \langle \boldsymbol{V}(\boldsymbol{a}_1,t)\cdot\boldsymbol{V}(\boldsymbol{a}_2,\tau)\rangle\,\mathrm{d}\tau = \langle \boldsymbol{V}(\boldsymbol{a}_1,t)\cdot\boldsymbol{A}(\boldsymbol{a}_2,t)\rangle.$$

Using the Cauchy–Schwarz inequality

$$|\Theta| \leqslant [\langle\|\boldsymbol{V}(\boldsymbol{a},t)\|^2\rangle_a]^{\frac{1}{2}}\cdot[\langle\|\boldsymbol{A}(\boldsymbol{a},t)\|^2\rangle_a]^{\frac{1}{2}}.$$

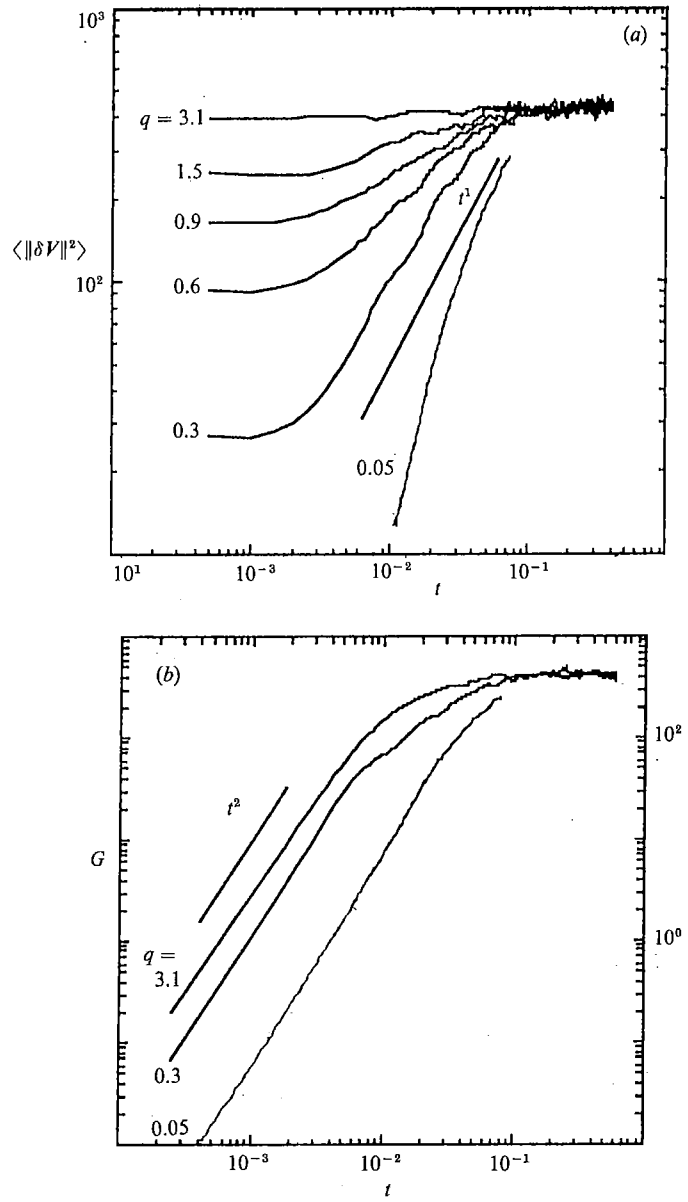

FIGURE 2. (*a*) Mean-squared relative velocity $\langle \|\delta V\|^2 \rangle$ and (*b*) G, as a function of time for various $q = D_0/D_I$.

The first term in the product refers to a mean Lagrangian energy and is therefore equal to $(2E)^{\frac{1}{2}}$; from (20)

$$|\Theta| \leqslant 2Et \quad \text{for} \quad n > 1$$

which, combined with (20) and (36), yields

$$0 \leqslant Y(t, D_0) \leqslant 8Et \quad \text{for} \quad n > 1,$$

or, after integrating in time,

$$0 \leqslant D^2(t, D_0) \leqslant D_0^2 + 8Et^2,$$

a weaker form of (35) extending to a frequency range where the Lagrangian energy

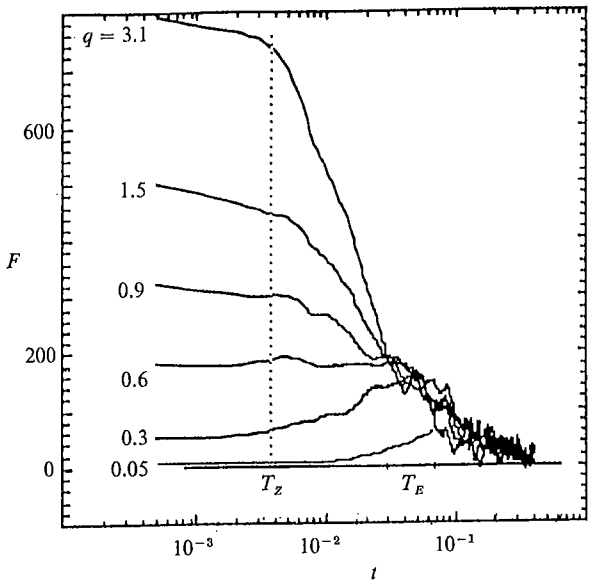

FIGURE 3. Time evolution of $F(t)$ for various $q = D_0/D_I$. Times T_Z and T_E (a function of D_0) are indicated.

spectrum is observed to be of the form ν^{-n} with $n > 1$, independently of the Eulerian spectral energy distribution. The experimental results presented in figure 1(*a*) and hereafter show that this time interval is perhaps better defined as $0 < t \leqslant T_Z$.

3.3. *Numerical experiments*

All the experimental results presented here come from the numerical simulations described in the Appendix, done with higher resolution than those of Babiano & Le Roy (1987); some of the conclusions of the former have to be slightly modified.

In figure 2 (experiments R256F40 and R1728F40) we plot for various values of the ratio $q = D_0/D_I$ the two terms $\langle \|\delta V\|^2 \rangle$ and G which contain the dynamics of the flow in equation (28) (the values of times T_I and T_E for these experiments can be estimated from figure 4*a*). The asymptotic behaviour (29) and (32) of $\langle \|\delta V\|^2 \rangle$ is well recovered: the curves start from levels which are an increasing function of q. They reach their common asymptotic level $4E$ after a growth phase whose slope varies between t^0 to t^b ($b > 1$). The asymptotic behaviour (31) and (33) of G is also experimentally well recovered. For $t \geqslant T_E$, the stationary stage $G = 4E$ has been reached.

Figure 3 (experiments R256F40 and R1728F40) shows the time evolution of the integrand $F(t)$ of (28) for various values of D_0. The curves clearly illustrate the fact that solution (28) is sensitive to D_0 for dispersion times $t < T_E$ (see Davis 1983) and that the asymptotic behaviour (35) is valid up to $t \approx T_Z$. From the physical standpoint, it is likely that $F(t)$ remains positive at all times for all values of D_0. Then, as $D_0 \to 0$, $F(t, D_0)$ must reach an asymptotic limit $F(t)$ which increases from zero to a maximum value in the vicinity of $t = T_E$, then decreases back to zero, with (29) and (31). This asymptotic limit for F is reached, in our experiments, for $q = 0.05$. It should be noticed that in this case behaviour (35) is valid up to $t \approx T_I$.

Figures 4(*a*) (experiments R256F40, R1024F40 and R1728F40) and 4(*b*) (experiment R1024F4) show the time evolution of D^2 plotted using a log-log scale.

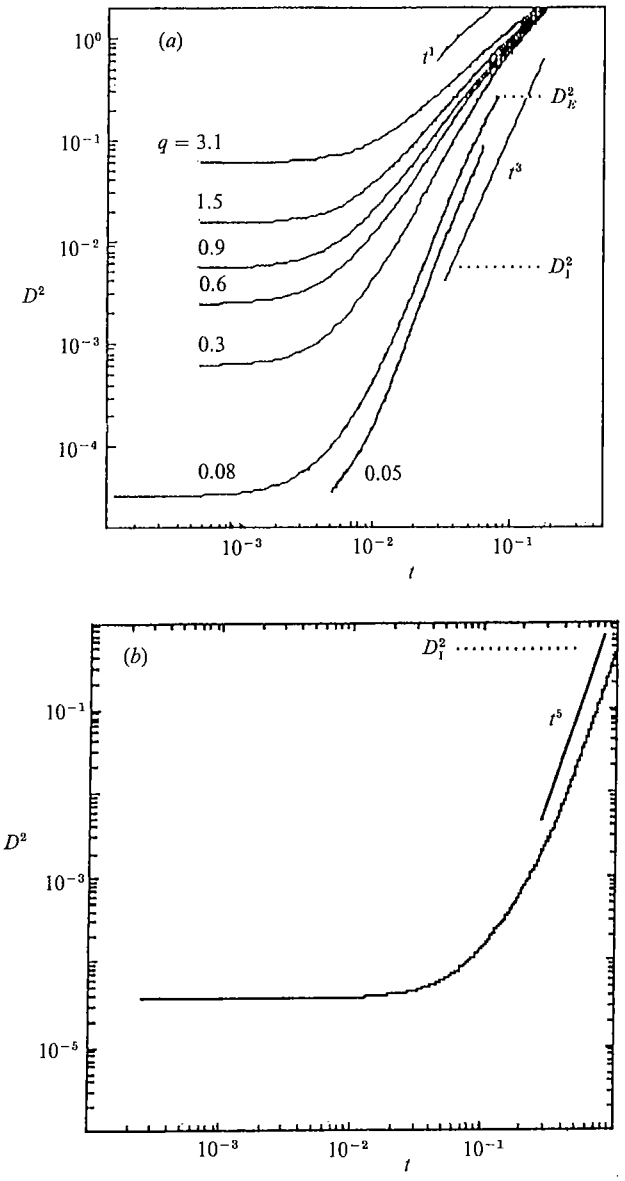

FIGURE 4. Relative dispersion as a function of time for various $q = D_0/D_I$; (*a*) experiments R256F40, R102F40 and R1728F40 ($0.05 \leqslant q \leqslant 3.1$); (*b*) experiment R1024F4 ($q = 0.008$). Scales D_I and D_E are indicated.

From the theory, we would expect a succession of four different types of behaviour: first, phase (35), followed by exponential growth K–L (2*b*) in the enstrophy inertial range, then a t^3 law R–O (2*a*) in the energy inertial range, and finally an asymptotic linear growth (30). But in fact we should remember that R–O and K–L are asymptotic laws which begin to be valid only when the observed separation scale is large enough compared to the separation scale D_0 at which the particle pairs have been released. In all our simulations, the initial behaviour (35) is well verified. Among all experiments displayed in figures 4(*a*) and 4(*b*), only the one in figure 4(*b*) shows a clear saturation of the dispersion law in the enstrophy inertial range ($D < D_I$). It

thus seems that the asymptotic law requires a value D/D_0 of the order of 30 to become established. We note however that the saturation law of $D^2(t)$ in figure 4(*b*) is a power law close to t^5, in contradiction to the predicted exponential of K–L. In the energy inertial range, the asymptotic t^3 prediction of R–O appears well verified for small enough values of the ratio $q = D_0/D_1$ (figure 4*a*). When the initial separation D_0 is not small, the growth of D^2 can be significantly slower than the t^3 law. This is consistent with the results described in Anikiev *et al.* (1985) and Okubo (1971) where $D^2 \sim t^a$ with $2 < a < 3$ was found for ratios q larger than 0.1. Note also that Kowalsky & Peskin (1981) have displayed numerical results similar to ours with q close to 0.3, in the framework of non-statistically stationary decaying turbulence. Lastly, the behaviour at long times displayed by our experiments (figure 4*a*) sustains the prediction of linear growth (30), reached for scales significantly larger than D_E, the most energetic scale.

To summarize, all theoretical predictions except the exponential law K–L have been sustained by our numerical experiments on the growth of relative dispersion. However, in the two inertial ranges, asymptotic laws can be reached only when the initial separation is small: the fact that we need a ratio D/D_0 roughly of the order of 30 to observe asymptotic laws there may be important when interpreting *in situ* measurements. In the following sections, we shall return to a more thorough discussion of R–O and K–L laws in order to investigate their limit of validity.

4. The 't^3 law'

4.1. *The stationarity hypothesis*

In a simplified approach to relations (26) and (27), we may assume, in addition to H1, the following hypotheses (Lin & Reid 1963):

$$\text{Hypothesis H2:} \quad \langle \delta \boldsymbol{V}_0 \cdot \delta \boldsymbol{V}(t) \rangle = 0,$$

$$\text{Hypothesis H3:} \quad \langle \delta \boldsymbol{\Gamma}(t) \cdot \delta \boldsymbol{\Gamma}(\tau) \rangle = R(\sigma), \quad \sigma = t - \tau.$$

With H2, the analysis of the primitive relations (26) and (27) is displaced to times for which the pairs of particles no longer retain the memory of their origin; it corresponds approximately to assuming $t > T_{\mathrm{L}}$. H3 supposes that the correlations of relative accelerations are statistically stationary, i.e. are functions only of $\sigma = t - \tau$. Note that hypothesis H3 was proposed by Lin & Reid for three-dimensional turbulence; in this case H3 is crude and inefficient in the energy range because for dispersion times long compared to T_{L} there is a high probability that scales larger than the energy inertial range have been attained. However, in two-dimensional turbulence H3 may be useful as scales in the inverse energy cascade ($D > D_{\mathrm{I}}$) are attained only for dispersion times large compared with T_{L}. Assuming H1–H3, relations $\langle \|\delta V\|^2 \rangle$ and G simplify to:

$$[\langle \|\delta V(t)\|^2 \rangle]_{\mathrm{H}} = \langle \|\delta V_0\|^2 \rangle + 2tI_0(t)\left[1 - \frac{1}{t}\frac{I_1(t)}{I_0(t)}\right], \tag{37}$$

$$[G(t)]_{\mathrm{H}} = \tfrac{2}{3}tI_0(t)\left[1 - \frac{3}{2t}\frac{I_1(t)}{I_0(t)} + \frac{1}{2t^3}\frac{I_3(t)}{I_0(t)}\right]; \tag{38}$$

where $$I_0(t) = \int_0^t R(\sigma)\,\mathrm{d}\sigma, \quad I_1(t) = \int_0^t \sigma R(\sigma)\,\mathrm{d}\sigma, \quad I_3(t) = \int_0^t \sigma^3 R(\sigma)\,\mathrm{d}\sigma,$$

and $[\cdot]_{\mathrm{H}}$ refers to H1–H3 hypotheses. Using (37) and (38), we get from (28)

$$D^2(t) = D_0^2 + \{\langle \|\delta V_0\|^2 \rangle + [G(t)]_{\mathrm{H}}\} t^2. \tag{39}$$

The interest of relation (39) is that it reformulates the exact dispersion problem (25) under the restrictive hypotheses H2 and H3 of Lin & Reid (1963) yielding the classical Richardson law R–O. Equations (39) and (28) are identical at small times (see (34)). This would seem to be a paradox, because at small times we expect the dispersion process to be non-stationary; however, the non-stationary terms omitted in (39) are then negligible. Following Lin & Reid, we may allow I_0 to converge for large time: $I_0(t) \sim$ const for $t_* < t < T_E$. It follows that

$$\frac{I_1(t)}{I_0(t)} = o(t), \quad \frac{I_3(t)}{I_0(t)} = o(t^3). \tag{40}$$

Then (37)–(39) yield the following behaviour:

$$[\langle \|\delta V(t)\|^2 \rangle]_{\mathrm{H}} \sim t, \quad [G(t)]_{\mathrm{H}} \sim t, \quad D^2(t) \sim t^3 \quad \text{when} \quad t > t_*. \tag{41}$$

The assumption that I_0 converges at some characteristic timescale t_* is reasonable if the Lagrangian time correlation of relative acceleration is indeed stationary; in that case the behaviour (41) would be only valid within the time span $t_* < t < T_E$, being replaced afterwards by the real asymptotics behaviour (29)–(31).

The experimental verification of H3 and (40) is conceivable only in the framework of numerical experiments. In all other cases the validity of H3 may only be tested *a posteriori* by checking whether (41) holds. Using (37)–(39) we get from (24) the following equation:

$$\frac{\mathrm{d}}{\mathrm{d}t} D^2 = [\langle \|\delta V_0\|^2 \rangle + \langle \|\delta V(t)\|^2 \rangle] t. \tag{42}$$

Equation (42) has been derived under hypotheses H2 and H3; it may be used then to verify the validity of these hypotheses. In that respect it has the advantage over relations (37)–(39) that all its terms are accessible to measurements. If we define the ratio

$$\Phi(t) = \frac{\mathrm{d}/\mathrm{d}t D^2}{[\langle \|\delta V_0\|^2 \rangle + \langle \|\delta V(t)\|^2 \rangle] t},$$

we already know that Φ is a decreasing function of t, vanishing for $t > T_E$ as $\mathrm{d}D^2/\mathrm{d}t$ becomes constant. The domain of validity of H2 and H3 will be determined by the region in which $\mathrm{d}D^2/\mathrm{d}t$ and its approximation (42) have the same growth law, i.e. $\Phi(t)$ exhibits a plateau.

4.2. *Numerical experiments*

Direct testing of the validity of (42) can be performed on the basis of the numerical experiments R1728F40. We plot in figure 5(*a*) the numerical values of both $\mathrm{d}D^2/\mathrm{d}t$ (curve 1) and its approximation (40) (curve 2). This is in fact equivalent to making a comparison between (42) and (24), as we have seen above that (24) is accurately verified in our numerical experiments (see Babiano & Le Roy 1987). The wrong estimation of dispersion by (42) as soon as t gets larger than T_{L} is conspicuous: there are apparently no intermediate times at which (42) would be valid. For example, for $t > 0.04$, i.e. in the time range where $D^2(t)$ reaches the t^3 regime seen in figure 4(*a*), the right-hand side (curve 2) and the left-hand side (curve 1) of (42) continue to diverge steadily from each other. This does not imply that H3 is invalid at that time. Indeed, the contribution of non-stationary terms is cumulative. Figure 5(*b*) shows

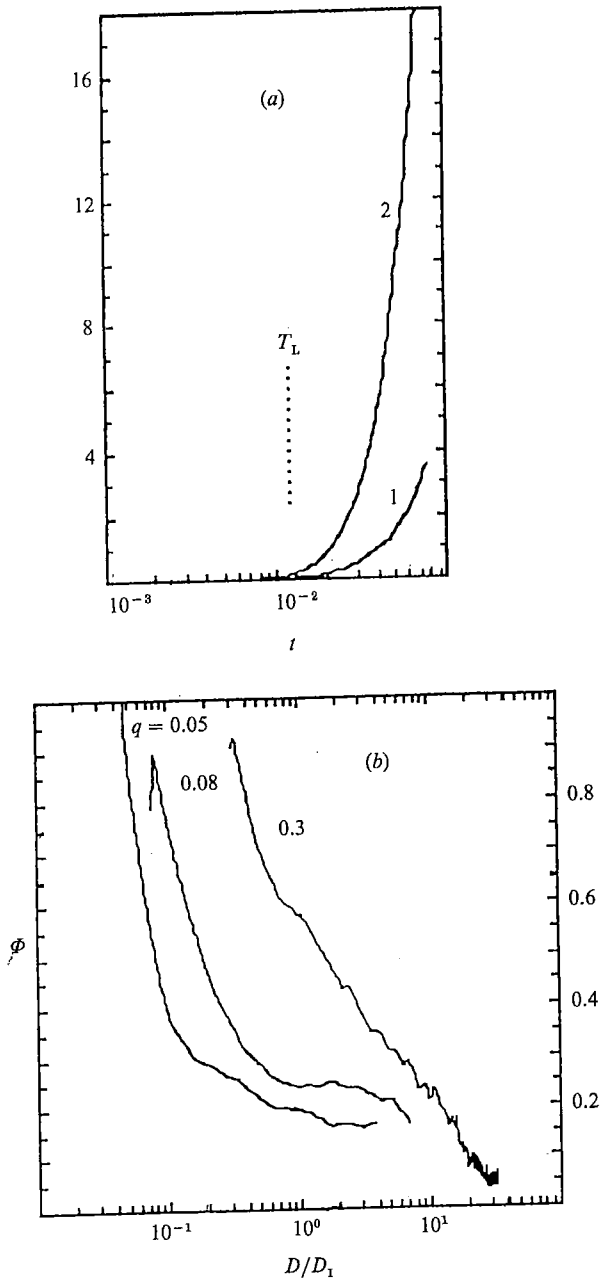

FIGURE 5. (*a*) Numerical values of both $\mathrm{d}D^2/\mathrm{d}t$ (curve 1) and its approximation (42) (curve 2) (experiment R1728F40); and (*b*) the D/D_I evolution of Φ (experiments R256F40, $q = 0.3$; R1024F40, $q = 0.08$; and R1728F40, $q = 0.05$).

evolution of the ratio Φ with D/D_I in the R256F40 ($q = 0.3$), R1024F40 ($q = 0.08$) and R1728F40 ($q = 0.05$) experiments. For $q = 0.3$ (no t^3 regimes, see figure 4*a*), Φ is decreasing over all the D/D_I range. For $q = 0.08$ and $q = 0.05$, Φ exhibits a plateau in the inverse energy cascade, where t^3 regimes have been observed (see figure 4*a*). These results show that there is a strong correlation between the t^3 growth and the pseudo-stationary regime within the inverse energy inertial range.

5. The 'exponential law'

5.1. *Characteristic time from relative dispersion*

By analogy with definition (16) for $\tau_X(\mathscr{D})$, we shall define the characteristic time of relative dispersion by

$$\tau_Y(t, D_0) = \frac{D^2(t, D_0)}{Y(t, D_0)}, \tag{43}$$

where $Y(t, D_0)$ is defined by (9). Within the limits of hypothesis H1 and relation (28), (43) can be rewritten

$$\tau_Y(t, D_0) = 2\frac{D_0^2 + t\int_0^t F(\tau, D_0)\,\mathrm{d}\tau}{tF(t, D_0) + \int_0^t F(\tau, D_0)\,\mathrm{d}\tau}. \tag{44}$$

Integrating (43) in time we get

$$D^2(t, D_0) = D_0^2 \exp\left[2\int_0^t \tau_Y^{-1}\,\mathrm{d}\tau\right]. \tag{45}$$

From (45) it is clear that the K–L law corresponds to the special case where the characteristic time τ_Y may be considered as locally constant. The time evolution of τ_Y is known from the relative dispersion asymptotic behaviour given in §§3.2, 3.3: at small times, τ_Y decreases from infinity, then it grows linearly with time for $t > T_E$. This behaviour has been qualitatively analysed by Batchelor (1952*b*) and Monin & Yaglom (1975). Between these two asymptotic types of behaviour, τ_Y passes through a minimum value corresponding to maximum efficiency of turbulent dispersion, reached when the angle between $\boldsymbol{D}$ and δV is minimum in the mean (see definition (9)).

Experimental results presented in figures 1 and 3 prove that the domain of validity of the asymptotic law (35), examined in §3.3, extends to times of order of T_Z. According to (35) we may rewrite the limited expansion of τ_Y. We get for $t \leqslant T_Z$:

$$D^2(t, D_0) = D_0^2 + 2S(D_0)\,t^2 + o(t^4), \tag{46}$$

where there is no t^3 term because its coefficient is proportional to $[\mathrm{d}/\mathrm{d}t\langle\|\delta V\|^2\rangle]_{t=0}$ which vanishes as shown by the experimental results displayed in figure 2. From (46) one gets

$$Y(t, D_0) = 2S(D_0)\,t + \alpha t^3 + o(t^4), \tag{47}$$

where $\alpha = Y'''(0, D_0)$. From (43), (46) and (47) we can derive the time dependency of τ_Y for $t \leqslant T_Z$:

$$\tau_Y = \frac{\tau_S^2(D_0) + \beta^2 t^2 + o(t^3)}{2t}, \tag{48}$$

with $$\beta = \left[2 - \frac{\alpha D_0^2}{2S^2(D_0)}\right]^{\frac{1}{2}} \quad \text{and} \quad \tau_S(\mathscr{D}) = \frac{\mathscr{D}}{(S(\mathscr{D}))^{\frac{1}{2}}}, \quad \mathscr{D} = \|D_0\|.$$

The structural time τ_S is an Eulerian characteristic. From BBS we know that in an enstrophy cascade range ($m \geqslant 3$), τ_S is constant and proportional to the inverse of the square root of enstrophy, so

$$\tau_S(D_0) \approx \sqrt{2}\,Z^{-\frac{1}{2}} = \sqrt{2}\,T_Z \quad \text{for} \quad D_0 < k_\mathrm{I}^{-1}. \tag{49}$$

According to (48) and (49) we see that τ_Y reaches a minimum value $\tau_{Y_{\min}} = \beta\tau_S(D_0)$ when $t = t_{\min} = \sqrt{2}\beta^{-1}T_Z$. Assuming (17):

$$\tau_{Y_{\min}} \approx \sqrt{2}\,\beta Z^{-\frac{1}{2}} = \frac{\beta}{\sqrt{2}}\tau_X, \tag{50}$$

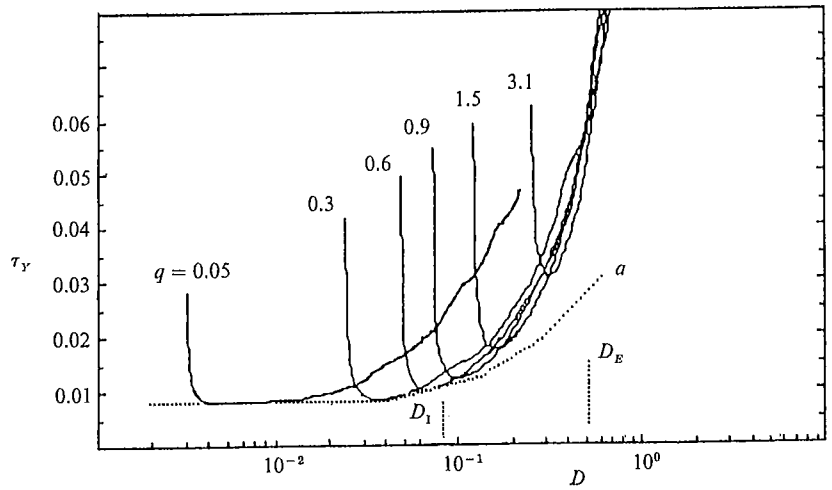

FIGURE 6. Characteristic time τ_Y as a function of D for various $q = D_0/D_I$ (experiments R256F40 and R1728F40); the dotted curve a corresponds to the function $\sqrt{2}\tau_S(D)$, which is equal to $\tau_X(D)$ in the enstrophy cascade range ($D < D_I$). Scales D_I and D_E are indicated.

with $\beta = \sqrt{2}$ when $\alpha = 0$. We observe that τ_Y is comparable with τ_X (i.e. $Y(D) = X(\mathscr{D} = D)$) only close to its minimum value (50).

Going further in the Taylor expansion of $(\tau_Y)^{-1}$ in the vicinity of $t_{\min}$:

$$\tau_Y^{-1}(t, D_0) = \tau_{Y_{\min}}^{-1} + \tfrac{1}{2}(t - t_{\min})^2 (\tau_Y^{-1})''_{t=t_{\min}} + o(t - t_{\min})^4. \tag{51}$$

Assuming (48), we may evaluate the second derivative at $(\tau_Y)^{-1}$ when $t = t_{\min}$:

$$(\tau_Y^{-1})''_{t=t_{\min}} = -\frac{\sqrt{2}}{8} T_Z^{-3}. \tag{52}$$

We obtain $\tau_Y^{-1}(t, D_0) \approx \tau_{Y_{\min}}^{-1}$ when $(t - t_{\min})^2 \ll \dfrac{2\tau_{Y_{\min}}^{-1}}{|(\tau_Y^{-1})''_{t=t_{\min}}|}$,

which yields

$$|t - t_{\min}| \ll \frac{2\sqrt{2}}{\beta^{\frac{1}{2}}} T_Z. \tag{53}$$

From this relation we may conclude that the exponential law K–L may be valid in the vicinity of $t_{\min}$ only for a duration of the order of T_Z.

5.2. *Experimental results*

Several characteristic times according to $D = (D^2(t))^{\frac{1}{2}}$ are displayed in figure 6: the experimental τ_Y defined by (43) and $\sqrt{2}\tau_S$ (curve a), which is equal to τ_X in the enstrophy cascade range ($D < D_I$) ($q = 0.05$ (R1728F40) and $0.3 \leqslant q \leqslant 3.1$ (R256F40)). The experimental τ_Y decreases from infinity to a minimum value. When D_0 is in the enstrophy range this minimum value is in excellent agreement with the theoretical result (49), (50) with $\alpha = 0$. When D_0 is in the reverse energy cascade range experimental results show that α cannot be neglected; because experimental minimum values of τ_Y are larger than theoretical values obtained with $\alpha = 0$ we conclude that, in our experiment, α is negative. After having reached its minimum, τ_Y departs rather quickly from τ_X, which means that the regime of exponential increase of D^2 is just a brief transient behaviour in the vicinity of $\tau_{Y_{\min}}$. When the initial separation scale lies at the bottom of the enstrophy inertial range (for

example, $q = 0.05$), the transient exponential behaviour ceases long before D_I is reached. In fact, we verify in all our experiments that it holds only in the close vicinity of $t = T_Z$; for $q = 0.05$, the observed duration of the exponential regime is 0.01, to be compared with a theoretical estimate of 0.0074, obtained from (53). The exponential regime is thus not an asymptotic law valid for $t \gg T_Z$, as assumed in Bennett (1984).

6. Conclusion

In this work we have examined, both numerically and theoretically, the statistical laws governing relative dispersion of particle pairs advected in a two-dimensional turbulent, incompressible, homogeneous and stationary velocity field. We obtained a rigorous differential equation governing relative dispersion. This differential equation, being based on simple kinematic relations between relative position, relative velocity and relative acceleration of particle pairs, is valid for both two- and three-dimensional dynamics. Concentrating on the incompressible two-dimensional case we focused our analysis on the classical Kraichnan–Lin and Richardson–Obukhov laws.

We found that, in dimension two, if the initial separation scale is small enough, dispersion has reached a quasi-stationary regime when it enters the scales of the energy inertial range: the t^3 law is then experimentally well verified and remains so up to the most energetic scales. We show that large-scale dispersion strongly depends on the initial separation D_0 of particles pairs. More precisely, in the time range when dispersion reaches the scales located between the forcing scale D_I and the most energetic scales, the time evolution of D^2 is close to t^3 only if the ratio $q = D_0/D_I$ is small enough. This behaviour was predicted long ago from self-similarity arguments. What is new in two-dimensional dynamics is that, for small enough D_0, the inverse energy inertial range is reached only after a long dispersion time, and then the contribution of non-stationary terms in the exact dispersion equation may have saturated. In that case the working assumption of stationarity and all its consequences may lead to analytical quantitative results valid for the inverse energy cascade of two-dimensional turbulence and comparable the Richardson–Obukhov law.

The Kraichnan–Lin law, on the other hand, is an approximation valid only near a characteristic configuration, already mentioned in Batchelor (1952*b*), where τ_Y is minimal. The minimum of τ_Y corresponds to the scale at which the turbulent diffusivity is most efficient, which itself depends on the initial separation scale; it is attained at a time of the order of T_Z. It is only because of the existence of this minimum, and in the vicinity of it, that D^2 obeys the exponential law: this behaviour occurs either in the energy inertial range, or in the enstrophy inertial range, depending on the initial separation scale. When it occurs in the enstrophy inertial range, it does not extend throughout to the injection scale; also in that case, we get $\tau_{Y_{\min}} = 2Z^{-\frac{1}{2}}$. The latter result, well verified in our experiments, allows an estimation of the enstrophy of the flow from dispersion measurements.

The numerical computations were performed under contract number 14004 of the Centre de Calcul Vectoriel pour la Recherche. The authors are grateful for constructive criticism by two referees, which led to improvement of the paper.

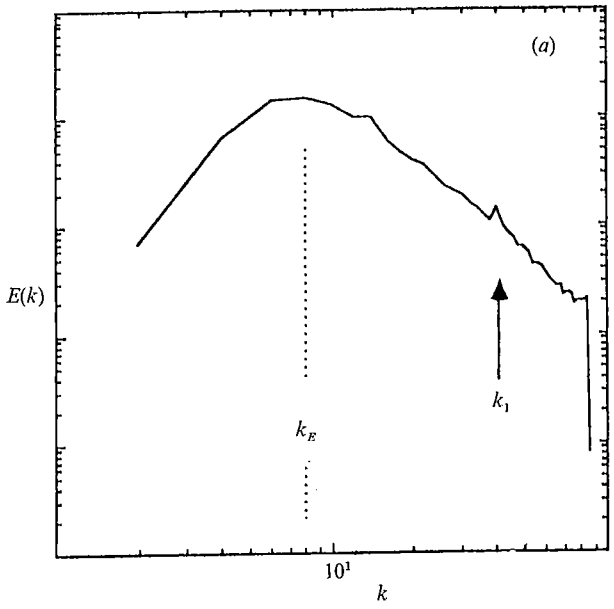

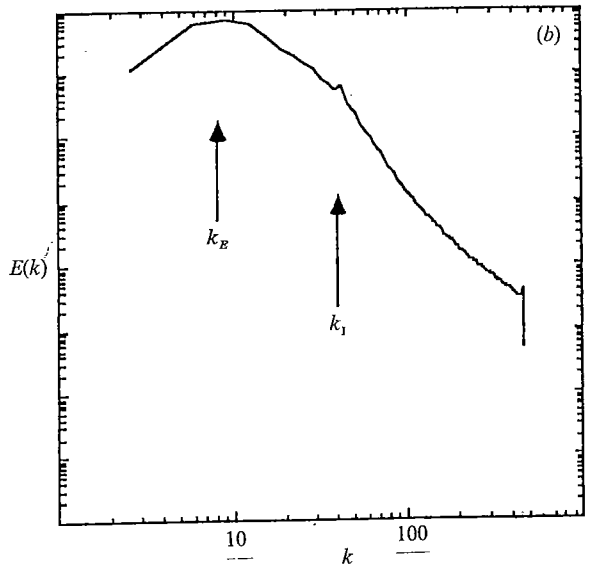

FIGURE 7 (*a*, *b*). For caption see facing page.

Appendix. The Eulerian numerical model and the Lagrangian experiments

In this work we use the Eulerian numerical simulation previously described in BBS and BBLS. The quasi-geostrophic barotropic vorticity equation

$$\frac{\partial \omega}{\partial t} + \mathrm{J}(\psi, \omega) = g(\omega) + f(\omega)$$

is integrated on a doubly periodic square domain of side L, using a pseudo-spectral

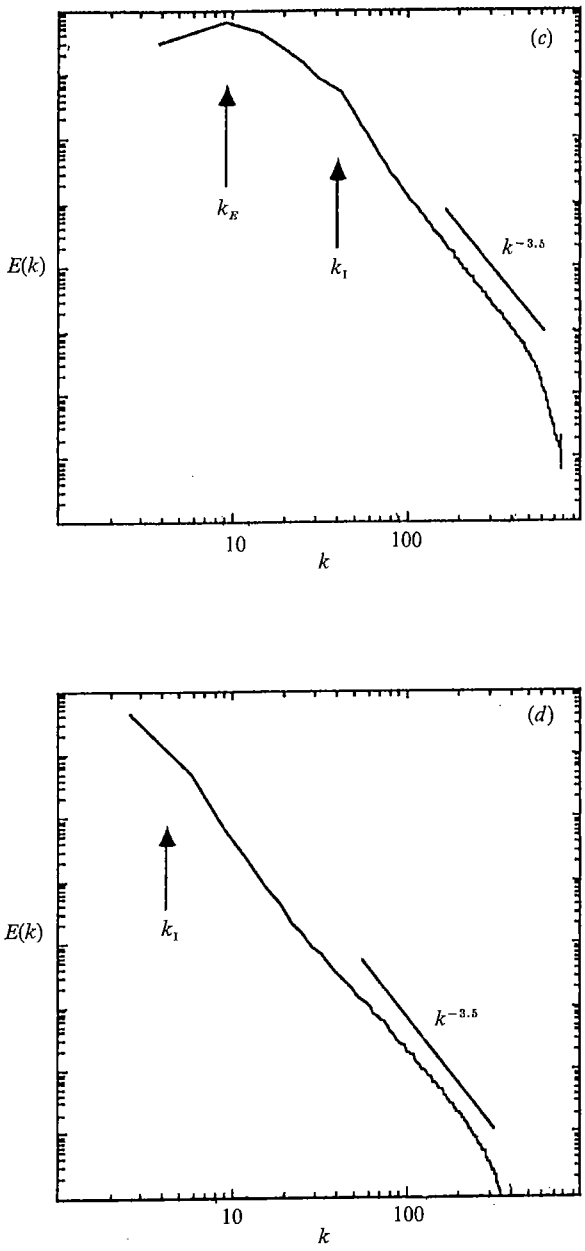

FIGURE 7. Eulerian energy spectrum. Arrows indicate the injection wavenumber $k_I = \pi/D_I$ and the most energetic wavenumber $k_E = \pi/D_E$; the resolutions used are: (*a*) 256^2, (*b*) 1024^2, (*c*) 1728^2, (*d*) 1024^2 for the F4 experiment (see Appendix); (log–log scale).

approximation (Basdevant *et al.* 1981) on 256^2, 1024^2 and 1728^2 grids. Here ψ refers to the stream function, ω to vorticity; $f(\omega)$ and $g(\omega)$ respectively to the forcing and dissipation terms and J the horizontal Jacobian. High resolutions, 1024^2 and 1728^2, were required to study relative dispersion $D^2(t)$ in the case of very small initial separation D_0. Except for the 1728^2 resolution, dissipation is defined as

$$g(\omega) = \mathrm{J}[\psi, \theta(l_c^2\Delta)^4\mathrm{J}(\psi,\omega)] + t_d^{-1}l_d^{-2}\psi,$$

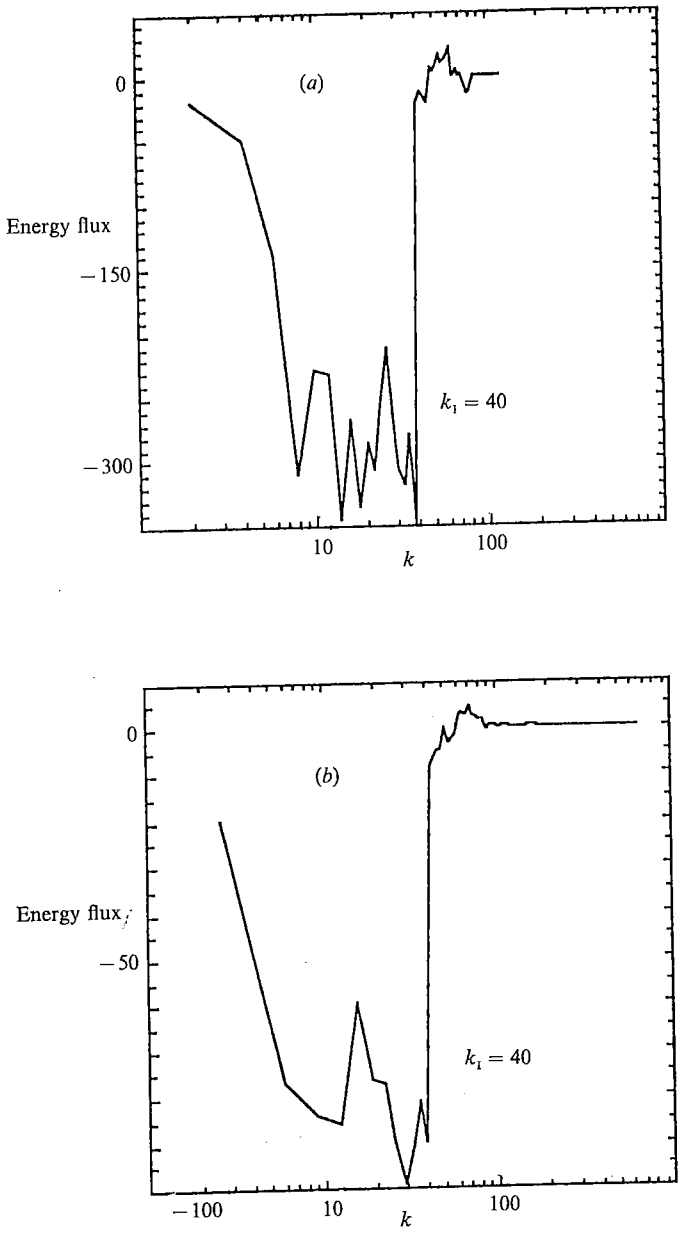

FIGURE 8. Energy fluxes; the resolutions used are (*a*) 256^2, (*b*) 1024^2; (log–log scale).

where θ and t_d are characteristic times, l_c the cutoff scale and l_d the largest scales. Dissipation thus involves a parameterization of subgrid scale called the 'anticipated potential vorticity method' (APVM) (Sadourny & Basdevant 1985), designed to dissipate only enstrophy near the cutoff scale, and a linear 'friction' to dissipate energy at larger scales. In experiments hereafter denoted F40, the forcing is defined by keeping the amplitude of the zonal mode $k_I = (0, 40)$ constant in time. In this way, even in the case of the 256^2 moderate resolution, we obtain a correct simulation of both the reverse energy and the direct enstrophy cascades because of the combined use of a large k_I and the APVM. This is illustrated by the Eulerian energy spectrum

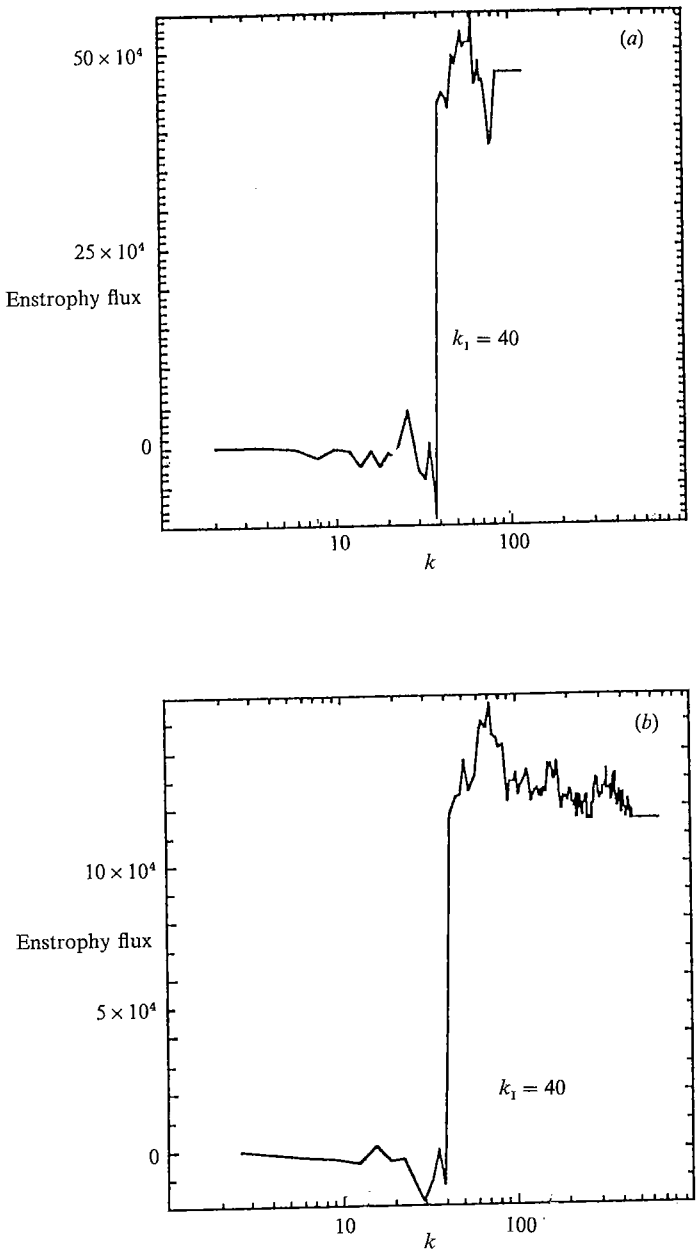

FIGURE 9. Enstrophy fluxes; the resolutions used are (*a*) 256^2, (*b*) 1024^2; (log–log scale).

(figures 7*a* and 7*b*) which behaves as $E(k) \sim k^{-m}$ on both sides of the injection wavenumber k_I, with an inertial enstrophy domain for $k > k_I$ ($m \geqslant 3$) and a reverse energy cascade for $k < k_I$ ($m \approx \frac{5}{3}$); this is also well illustrated by the constancy of energy (figures 8*a* and 8*b*) and enstrophy (figures 9*a* and 9*b*) fluxes.

In the case with a resolution of 1728^2, we use the dissipation

$$g(\omega) = -t_c^{-1}(-l_c^{-1}\Delta)^8\omega + t_d^{-1}l_d^{-2}\psi$$

described in BBLS, where t_c is another characteristic time. The iterated Laplacian

(Basdevant *et al.* 1983) used here to dissipate essentially enstrophy near the cutoff scale is not as efficient as the APVM described above in simulating the dynamics of the very small scales; but the APVM would have required too much memory.

These F40 experiments with various resolutions (R256F40, R1024F40 and R1728F40) can be compared easily to one another because all are scaled with the same forcing scale; the results of the three different resolutions used are displayed together on figure 4(*a*) ($0.05 \leqslant q \leqslant 3.1$). In one further F4 experiment (R1024F4) the forcing is applied on a smaller zonal mode $k_{\mathrm{I}} = (0, 4)$ with a 1024^2 grid. With this choice we obtain a very wide enstrophy inertial range (see figure 7*d*), which allows us to perform relative dispersion experiments with very small values of the ratio q ($q = 0.008$).

The Lagrangian motion is obtained by integrating the transport equation

$$\frac{\mathrm{d}\boldsymbol{X}}{\mathrm{d}t} = \boldsymbol{V}(\boldsymbol{X}, t)$$

using a Runge–Kutta second-order scheme (RK2):

$$\boldsymbol{X}_1 = \boldsymbol{X}(t) + \Delta t\, \boldsymbol{V}(\boldsymbol{X}, t),$$

$$\boldsymbol{X}(t + \Delta t) = \boldsymbol{X}(t) + \tfrac{1}{2}\Delta t[\boldsymbol{V}(\boldsymbol{X}, t) + \boldsymbol{V}(\boldsymbol{X}_1, t)],$$

where Δt is the time step of the Eulerian model. $\boldsymbol{V}(\boldsymbol{X}, t)$ and $\boldsymbol{V}(\boldsymbol{X}_1, t)$ are evaluated by linear interpolation within a mesh. The truncation error was investigated in great detail in BBLS in the case of an Euler advection scheme. Here the RK2 scheme used is more precise. The two schemes are compared: the quantity displayed is the squared displacement $A^2(t)$ of one particle advected around a strong vortex in a frozen field (i.e. an Eulerian field which does not change in time). In the Euler case, $A^2(t)$ never comes back to zero and increases in mean: this indicates that the trajectory is not circular but spiral. In the RK2 case the displacement vector regularly comes back to zero. The individual particle has turned around the vortex more than ten times on exactly the same trajectory as expected in a frozen field. This clearly indicates that with the RK2 scheme the numerical diffusion, which in BBLS was essentially noticed in the vicinity of the vortices, has become quite negligible. A more accurate time scheme (RK4) together with a spline interpolation, ensuring the continuity of the Lagrangian acceleration field, did not modify significantly the statistical results of the present work (N. Zouari, private communication).

At stationary regime conditions ($Z(t) \approx$ const. and $E(t) \approx$ const.), a set of 1024 pairs of particles for experiments R256F40 (4096 pairs for experiments R1024F40, R1024F4 and R1728F40) all with the same separation ($D_0 = i\Delta x$, where Δx is the grid interval and $i = 1, 2, 3, 5, 10$) are released all over the entire domain and statistics leading to evaluation of mean relative dispersion are constructed for several values $q = D_0/D_{\mathrm{I}} = i\Delta x/D_{\mathrm{I}}$. Characteristic non-dimensional parameters of our experiments are displayed in table 1. The scale factors l^* and t^* used to non-dimensionalize the equations were obtained by prescribing the forcing scale d_{I} ($d_{\mathrm{I}} = 50$ km) and the mean energy e ($e = 8$ cm^2 s^{-2} for F4 and $e = 200$ cm^2 s^{-2} for F40). Times T_{I} and T_E, as a function of q, can be estimated easily from figures 4(*a*) and 4(*b*).

REFERENCES

Anikiev, V. V., Zaytsev, O. V., Zaytseva, T. V. & Yarosh, V. V. 1985 Experimental investigation of the diffusion parameters in the ocean. *Izv. Atmos. Ocean Phys.* **21**, 931–934.

BABIANO, A., BASDEVANT, C., LE ROY, P. & SADOURNY, R. 1987 Single-particle dispersion, Lagrangian energy spectrum in two-dimensional incompressible turbulence. *J. Mar. Res.* **45**, 107–131 (referred to as BBLS).

BABIANO, A., BASDEVANT, C. & SADOURNY, R. 1985 Structure functions and dispersion laws in two-dimensional turbulence. *J. Atmos. Sci.* **42**, 942–949 (referred to as BBS).

BABIANO, A. & LE ROY, P. 1987 Quelques remarques sur la formulation non autosimilaire des lois de dispersion relative en turbulence bidimensionnelle. *C.R. Acad. Sci. Paris* **305**, II, 5–8.

BASDEVANT, C., LEGRAS, B., SADOURNY, R. & BÉLAND, M. 1981 A study of barotropic model flows: Intermittency waves and predictability. *J. Atmos. Sci.* **38**, 2305–2326.

BATCHELOR, G. K. 1952*a* Diffusion in field of homogeneous turbulence. II. The relative motion of particles. *Proc. Camb. Phil. Soc.* **48**, 345–362.

BATCHELOR, G. K. 1952*b* The effect of homogeneous turbulence on material lines and surfaces. *Proc. R. Soc. Lond.* A **213**, 349–366.

BENNETT, A. F. 1984 Relative dispersion: Local and non-local dynamics. *J. Atmos. Sci.* **41**, 1881–1886.

BENNETT, A. F. 1987 A Lagrangian analysis of turbulent diffusion. *Rev. Geophys.* **25**, 799–822.

DAVIS, R. E. 1983 Oceanic property transport, Lagrangian particle statistics, and their prediction. *J. Mar. Res.* **41**, 163–194.

ER-EL, J. & PESKIN, R. L. 1981 Relative dispersion of constant-lebel balloons in the Southern Hemisphere. *J. Atmos. Sci.* **38**, 2264–2274.

HINZE, J. O. 1975 *Turbulence.* McGraw-Hill. 790 pp.

KOWALSKI, A. D. & PESKIN, R. L. 1981 Numerical simulation of relative dispersion in two-dimensional, homogeneous, decaying turbulence. *J. Fluid Mech.* **109**, 45–61.

KRAICHNAN, R. H. 1966 Dispersion of particle pairs in homogeneous turbulence. *Phys. Fluids* **9**, 1937–1943.

LIN, C. C. 1960 On a theory of dispersion by continuous movements. *Proc. Natl Acad. Sci. USA* **46**, 566.

LIN, C. C. & REID, W. H. 1963 Turbulent flow. Theoretical aspects. In *Handbuch der Physik*, vol. VIII/2. Springer.

LIN, J. T. 1972 Relative dispersion in the enstrophy cascading inertial range of homogeneous two-dimensional turbulence. *J. Atmos. Sci.* **29**, 394–396.

MONIN, A. S. & YAGLOM, A. M. 1975 *Statistical Fluid Mechanics.* The MIT Press. 874 pp.

MOREL, P. & LARCHEVÊQUE, M. 1974 Relative dispersion of constant level balloons in the 200 mb general circulation. *J. Atmos. Sci.* **31**, 2189–2195.

OBUKHOV, A. M. 1941 Energy distribution in the spectrum of turbulent flow. *Izv. Akad. Nauk. SSSR, Ser.-Geogr. i Geofiz.* **5**, 453–466.

OKUBO, A. 1971 Oceanic diffusion diagrams. *Deep-Sea Res.* **18**, 789–802.

PRICE, J. 1981 Diffusion statistics computed from SOFAR float trajectories in the western North Atlantic. *CAMS-WHOI Symposium on Lagrangian tracers. Woods Hole, March, 1981,* unpublished proceedings.

SADOURNY, R. & BASDEVANT, C. 1985 Parameterization of subgrid scale barotropic eddies in quasi-geostrophic models: anticipated potential vorticity method. *J. Atmos. Sci.* **42**, 1353–1363.